DOI: 10.19884/j.1672-5220.202507001

Medium-Entropy $(Zr_{1/3}Hf_{1/3}W_{1/3})C$ Ceramic Toughened by In-Situ-Formed Silicon Carbide via Low-Temperature Reactive Spark Plasma Sintering

LI Mengfei, PENG Pai, LIU Jixuan*, QIN Yuan, CHENG Weiqiang, ZHANG Guojun
State Key Laboratory of Advanced Fiber Materials, College of Materials Science and Engineering, Donghua University, Shanghai 201620

Abstract: Medium-entropy transition metal carbide ceramics and their composites are important materials for extreme environments. However, they face challenges in densification difficulties and low fracture toughness. To address this issue, a medium-entropy ceramic powder with a nominal composition of $(Zr_{1/3}Hf_{1/3}W_{1/3})C$ (MEC) was synthesized by carbothermal reduction. Then, silicon (Si) was added, and the reactive spark plasma sintering (RSPS) technology was used to prepare MEC-based composite ceramics. The results show that MEC ceramics without Si addition can only form a single-phase solid solution when sintered at 1 900 ℃, with a relative density of 96.7% and an average grain size of (3.8 ± 1.3) μm. By adding 5% Si by mass, the MEC-based composite ceramic with a relative density of 98.8% can be obtained by sintering at a relatively low temperature of 1 700 ℃. It is composed of an MEC solid solution phase and an in-situ-formed silicon carbide (SiC) secondary phase, and the average grain size of the MEC matrix phase is only (1.4 ± 0.3) μm. Compared with the single-phase MEC ceramic, the fracture toughness of the MEC-based composite ceramic prepared by adding Si increases by 24.8% to (3.42 ± 0.24) MPa·m$^{1/2}$. It is considered that Si, with a low melting point, can form a liquid phase during sintering, promoting densification. Additionally, the reaction between Si and carbide results in the formation of carbon vacancies in the latter, which can accelerate atomic diffusion and promote the formation of the MEC solid solution phase. In addition, the in-situ-formed SiC not only pins the grain boundaries of the matrix phase to hinder its growth, but also causes crack deflection to improve the fracture toughness of materials. The research results can provide references for the design and preparation of novel medium-entropy carbide-based ceramics for extreme environments.

Keywords: medium-entropy carbide; carbothermal reduction; reactive sintering; silicon carbide; toughening
CLC number: TB321 **Document code**: A
Article ID: 1672-5220(2026)02-0051-08

Open Science Identity (OSID)

0 Introduction

Transition metal carbides of Groups IVB-VIB, such as ZrC and HfC, have emerged as critical high-temperature structural materials for aerospace and advanced nuclear energy applications due to their high melting points, high Young's modulus, and excellent oxidation and ablation resistance[1-4]. However, as aerospace technology advances toward much higher temperatures, coupled with escalating demands for safety and efficiency in nuclear power systems, the comprehensive performance requirements for these carbides have become increasingly stringent. In recent years, the entropy engineering modification strategy has opened up new avenues for enhancing transition metal carbides[5-18]. This approach revolutionizes the traditional paradigm of material design by introducing multiple principal elements into crystal lattice sites with random occupancy, forming medium-entropy solid solutions with configurational entropy ΔS falling within the range of $0.69R$ to $1.50R$ ($R = 8.314$ J/(mol·K)) and high-entropy solid solutions with $\Delta S > 1.50R$, respectively. It not only enables the synergistic optimization of multiple properties but also allows for the customizable design of medium- to high-entropy carbides and their composites with tailored characteristics.

Castle et al.[5] reported the synthesis of rock-salt structured high-entropy (Hf, Ta, Zr, Ti)C and (Hf, Ta, Zr, Nb)C ceramics via high-energy ball milling combined with spark plasma sintering (SPS) at 2 300 ℃. The Vickers hardness of (Hf, Ta, Zr, Nb)C reached 36.1 GPa, exceeding the rule-of-mixtures (ROMs) prediction by about 30%. Li et al.[13] systematically investigated (Nb, Ta, Zr)C, (Nb, Ta, Zr, Hf)C, (Nb, Ta, Zr, W)C, and (Nb, Ta, Zr, Hf, W)C systems, revealing that the ternary medium-entropy (Nb, Ta, Zr)C ceramic exhibited the highest sintered density alongside the superior Young's modulus and hardness. Zhang et al.[14] compared the mechanical

Received date: 2025-07-05
Foundation items: National Natural Science Foundation of China (Nos. 52371023 and 52032001)
* Correspondence should be addressed to LIU Jixuan, email: jxliu@dhu.edu.cn
Citation: LI M F, PENG P, LIU J X, et al. Medium-entropy $(Zr_{1/3}Hf_{1/3}W_{1/3})C$ ceramics toughened by in-situ-formed silicon carbide via low-temperature reactive spark plasma sintering [J]. *Journal of Donghua University (English Edition)*, 2026, 43(2): 51-58.

properties of unary and multicomponent transition metal carbides, confirming that ternary medium-entropy carbides outperform high-entropy carbides and quaternary medium-entropy carbides in Young's modulus.

Current studies indicate that medium-entropy carbides often exhibit superior properties compared to high-entropy carbides (HECs), showing significant potential in aerospace and nuclear applications[12-13,19-21]. Nevertheless, medium-entropy carbides still face the fundamental challenges inherent to traditional transition metal carbides: difficult densification and low fracture toughness. Sintering temperatures for medium-entropy carbides typically range from 1 900 ℃ to 2 100 ℃, often resulting in coarse microstructures and degraded mechanical properties. Even high-performance ternary medium-entropy carbides like (Nb, Ta, Zr)C exhibit limited fracture toughness (2.9–3.1 MPa·$m^{1/2}$)[13, 21], falling below that of some conventional engineering ceramics. This severely hinders their development and application. Thus, achieving enhanced densification and fracture toughness is critical to overcoming practical application barriers for medium-entropy carbides.

Previous studies on conventional transition metal carbides demonstrate that Si addition can simultaneously reduce sintering temperatures, refine microstructures, and improve fracture toughness. For example, Wang et al.[22] utilized reactive hot pressing of ZrC and Si to lower the densification temperature from 1 900 – 2 000 ℃ to 1 600 ℃, achieving dense ZrC ceramics with relative densities higher than 98%. During sintering, ZrC reacted with Si to form ZrC_{1-x} and SiC. The in-situ-formed SiC secondary phase induced crack deflection during fracture, dissipating energy and increasing fracture toughness to 3.3 MPa·$m^{1/2}$, which is 73.7% higher than that of monolithic ZrC. Theoretically, this strategy can also be effective for medium-entropy carbides, because they have similar physical and chemical properties. Compared to hot pressing, SPS offers rapid heating, short dwell time, lower sintering temperature, and superior grain growth suppression[21-27]. Therefore, combining reactive sintering with SPS to prepare medium-entropy carbide-based ceramics, using medium-entropy carbide and Si powders as the starting material, should enable low-temperature densification and mechanical enhancement of this material. However, no such studies have been reported. Notably, the complex multi-element nature of medium-entropy carbides may lead to more intricate reactions with Si than in unary systems, such as ZrC. Whether the Si-addition strategy remains effective for medium-entropy carbides still requires experimental validation. To address this gap, the present work proposes using Si as a sintering additive and reactive spark plasma sintering (RSPS) for low-temperature densification and toughening of medium-entropy carbides. Zr, Hf, and W are selected as constituent elements for the medium-entropy carbide for the following reasons. First, ZrC and HfC are typical ultra-high-temperature ceramics renowned for their exceptional melting points, Young's modulus, and stability in extreme environments, while WC exhibits exceptional hardness and high wear resistance. Incorporating Zr, Hf, and W thus holds promise for the medium-entropy carbide to inherit these advantageous properties. Second, previous work has demonstrated that incorporating W and/or Hf into Nb-Ta-Zr-based medium-entropy carbides significantly increases fracture toughness by 30% – 45%[13]; consequently, W and Hf are specifically selected to address the inherent brittleness of carbides in this study. Third, the differences in atomic radii among Zr (0.160 nm), Hf (0.159 nm), and W (0.139 nm) are expected to induce severe lattice distortion, thereby enhancing the hardness of the medium-entropy carbide. Therefore, by using ZrO_2, HfO_2, WO_3, and carbon black as raw materials, the medium-entropy carbide ceramic powder with a nominal composition of $(Zr_{1/3}Hf_{1/3}W_{1/3})C$ (MEC) and a theoretical ΔS value of $1.1R$ was synthesized via carbothermal reduction. The effects of Si addition on the phase composition, density, microstructure, and mechanical properties of MEC-based ceramics prepared by RSPS were investigated to provide insights for designing and fabricating advanced MEC-based ceramics for extreme environments in aerospace and nuclear energy applications.

1 Materials and Methods

1.1 Synthesis of MEC powder

MEC powder was synthesized via carbothermal reduction by using zirconium dioxide (ZrO_2, purity higher than 99.95%, a particle size of approximately 0.2 μm, Dongguan Surpass Structural Ceramics Co., Ltd., China), hafnium dioxide (HfO_2, purity higher than 99.95%, a particle size of approximately 0.1 μm, Found Star Science and Technology Co., Ltd., China), tungsten trioxide (WO_3, purity higher than 99.95%, a particle size of approximately 0.1 μm, Zhuzhou Cemented Carbide Group Co. Ltd., China), and carbon black (purity higher than 99.9%, a particle size of approximately 40 nm, Alfa Aesar, China) as raw materials. The starting powders were weighed according to the stoichiometric ratio of Reaction (1) and loaded into a 500 mL polyethylene jar containing ZrO_2 grinding balls with a ball-to-powder mass ratio of 3∶1.

$$ZrO_2 + HfO_2 + WO_3 + 10C \rightarrow 3(Zr_{1/3}Hf_{1/3}W_{1/3})C + 7CO(g). \quad (1)$$

Anhydrous ethanol was used as the dispersant. The powder mixing was conducted on a roller mixer at 120 r/min for 10 h. Then, the achieved slurry was evaporated by using a rotary evaporator to remove ethanol, followed by drying in an oven at 60 ℃ for 10 h. The dried powder mixture was placed in a graphite crucible and heated at 1 700 ℃ for 1 h in a vacuum sintering furnace (ZT-15-

20, Shanghai Chenhua Electric Furnace Co., China) under vacuum. The heating rate is 10 ℃/min. The synthesized carbide powder was manually ground and sieved through a 200-mesh screen.

1.2 Preparation of MEC-based ceramics

The Si powder (purity higher than 99.6%, particle size less than 45 μm), 5% by mass (hereafter referred to as 5% Si), was added to the as-synthesized MEC powder. The MEC/Si mixed powder was obtained through the same mixing and drying processes described above, and then loaded into a graphite mold. The mold was placed in an SPS furnace and sintered under an argon atmosphere at a heating rate of 100 ℃/min to 1 500 ℃ and 1 700 ℃, respectively. After holding at the sintering temperatures of 1 500 ℃ and 1 700 ℃ for 10 min under an axial pressure of 40 MPa, respectively, the MEC-based ceramics designated as MEC-5Si-1500 and MEC-5Si-1700 were prepared. Meanwhile, by using the above-mentioned sintering process, Si-free MEC ceramics were prepared at 1 500, 1 700, and 1 900 ℃ as reference samples, labeled as MEC-0Si-1500, MEC-0Si-1700, and MEC-0Si-1900, respectively. All samples were subjected to cutting, grinding, and polishing for subsequent characterization and property measurements.

1.3 Sample characterization

Phase composition and lattice parameters of samples were determined by X-ray diffraction (XRD) patterns obtained from Bruker D2 Phaser (Cu Kα radiation, λ = 0.154 2 nm, 30 kV, 10 mA). Thermodynamic analysis of the powder synthesis process was performed by using HSC Chemistry 6.1 software. Theoretical densities of the prepared samples were calculated based on the measured lattice parameters, the theoretical mass of the crystal cell, and the nominal phase contents. Bulk densities of the ceramic samples were measured by using the Archimedes method, and relative densities were derived from the ratio of bulk density to the theoretical density. The microstructure of the samples was examined by a scanning electron microscope (MAIA 3, TESCAN, the Czech Republic). At the same time, elemental distribution was analyzed via energy-dispersive X-ray spectroscope (EDS) (SU8220, Hitachi, Japan). Average grain sizes for each phase (no less than 200 grains per phase) were statistically quantified from scanning electron microscopy (SEM) images by using ImageJ software. Young's modulus E of the sintered ceramics was measured by using the UMS-100 ultrasonic system. Vickers hardness $H_{V1.0}$ was tested at a load of 9.8 N with a dwell time of 15 s by using the HXD-1000TM/LCD hardness tester (Shanghai Taiming Optical Instrument Co., Ltd., China). The fracture toughness K_{IC} of the sintered sample was evaluated via the indentation method, and it was calculated by

$$K_{IC} = 0.016\,(E/H_{V5.0})^{1/2}\,P\,c^{-3/2},$$

where $H_{V5.0}$ is the Vickers hardness (unit: GPa) measured by using indentation load P of 49 N; c is half-length of the indentation diagonal (unit: mm). The reported values for E, $H_{V5.0}$, and K_{IC} represent averages of five independent measurements.

2 Results and Discussion

2.1 Phase composition and microstructure of the synthesized MEC powder

Figure 1 presents the SEM morphology and XRD pattern of the synthesized MEC powder. The powder exhibits fine particles with an average size of about 150 nm (Fig. 1(a)). XRD analysis reveals that the synthesized MEC is not a single-phase solid solution. Instead, it consists primarily of incompletely homogenized cubic carbide solid solutions with a minor hexagonal WC phase (Fig. 1(b)), indicating an uncompleted solid solution formation. It can be attributed to the differences in the thermodynamic driving forces for carbothermal reduction of distinct oxide precursors (ZrO_2, HfO_2, and WO_3) and the crystal structure incompatibility between hexagonal WC and cubic MEC phases.

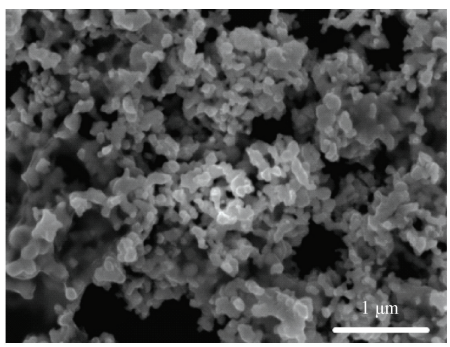

(a)

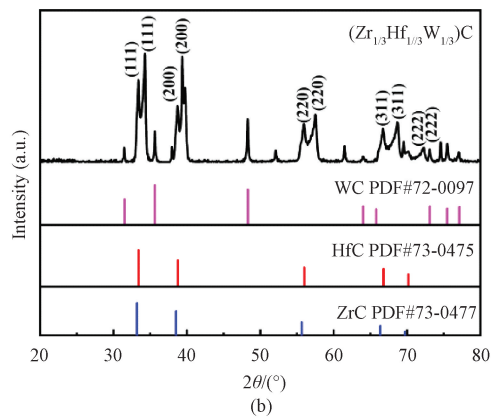

(b)

Fig. 1 Microstructure and phase composition of the synthesized MEC powder: (a) SEM morphology; (b) XRD patterns

Theoretically, the overall carbothermal reduction reaction in this synthesis system, i. e., Reaction (1) mentioned previously, can be decomposed into the following elementary reactions:

$$ZrO_2+3C\rightarrow ZrC+2CO(g), \quad (2)$$

$$HfO_2+3C\rightarrow HfC+2CO(g), \quad (3)$$

$$WO_3+4C\rightarrow WC+3CO(g), \quad (4)$$

$$ZrC+HfC+WC\rightarrow 3(Zr_{1/3}Hf_{1/3}W_{1/3})C. \quad (5)$$

Figure 2 plots the temperature dependence of the standard Gibbs free energy ΔG° for Reactions (2)–(4). Obviously, ΔG° values for Reactions (2)–(4) are negative at the synthesis temperature of 1 700 ℃ (Fig. 2), confirming the thermodynamic feasibility of complete oxide-to-carbide conversion. Crucially, Reaction (4), which represents carbothermal reduction of WO_3, achieves a negative ΔG° above 630 ℃, whereas Reactions (2) and (3) require temperatures higher than 1 650 ℃ to get a negative ΔG°. This suggests that WC likely forms prior to ZrC and HfC at lower temperatures during powder synthesis, followed by MEC solid solution formation via Reaction (5), rather than through a direct one-step synthesis process via Reaction (1). Moreover, the fundamental crystal structure mismatch between hexagonal WC and cubic ZrC/HfC significantly increases the energy barrier for their mutual solid solution formation, which hinders the complete progression of Reaction (5), ultimately resulting in the retention of the minor hexagonal WC phase in the synthesized MEC powder.

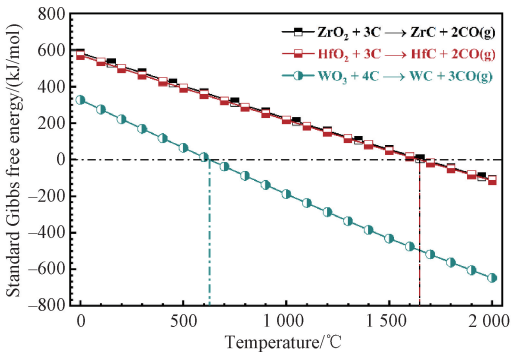

Fig. 2 Variation of standard Gibbs free energy with temperature for carbothermal reduction reaction of transition metal oxides under standard conditions

2.2 Phase composition, relative density, and microstructure of MEC-based ceramics

2.2.1 Phase composition of MEC-based ceramics

Figure 3 displays XRD patterns of MEC-based ceramics sintered at 1 700 ℃ and 1 900 ℃. Compared to the as-synthesized multiphase carbide powder, the ceramic, MEC-0Si-1700, retained its multiphase nature, whereas MEC-0Si-1900 exhibited a single-phase structure with a face-centered cubic (FCC) arrangement. This confirms that the elevated sintering temperatures promote solid solution formation, with residual hexagonal WC in the synthesized carbide powder fully dissolving into the FCC MEC phase at 1 900 ℃. Notably, adding 5% Si enabled the formation of a dual-phase MEC/SiC composite (MEC-5Si-1700) at 1 700 ℃, with no detectable WC phase. Obviously, Si addition accelerates the dissolving of residual WC into the FCC structured MEC matrix at a low sintering temperature. This can be attributed to the following mechanism: Si reacts with the synthesized MEC powder, generating SiC and inducing abundant carbon vacancies in the MEC matrix during sintering through Reaction (6):

$$(Zr_{1/3}Hf_{1/3}W_{1/3})C+xSi\rightarrow(Zr_{1/3}Hf_{1/3}W_{1/3})C_{1-x}+xSiC. \quad (6)$$

High-concentration carbon vacancies can promote atomic diffusion within the carbide lattice, facilitating the dissolution of the residual WC phase in the as-synthesized powder into the MEC matrix phase. Moreover, prior studies confirm that carbon vacancies significantly alter lattice parameters in transition metal carbides[26-27]. In this work, the lattice constants of the MEC phase in MEC-0Si-1900 and MEC-5Si-1700 are 0.455 74 and 0.460 25 nm, respectively, indicating a 1% increase in lattice parameter and 3% expansion in the volume of the MEC phase in Si-modified samples compared to samples prepared without Si addition.

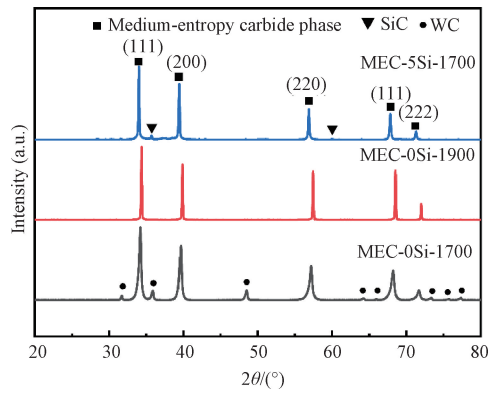

Fig. 3 XRD patterns of MEC-based ceramics

2.2.2 Relative densities of MEC-based ceramics

Figure 4 shows the bulk density and relative density of MEC-based ceramics sintered at different temperatures. Obviously, for both Si-free and Si-added samples, the bulk density and relative density increase with the rise of sintering temperature. For Si-free samples, a relative density of 91.7% is achieved at 1 700 ℃, but near-full densification with a relative density of 96.7% is realized at 1 900 ℃. In contrast, adding 5% Si significantly accelerates the densification. MEC-5Si-1700 shows a high relative density of 98.8%. The results indicate that the addition of Si effectively promotes low-temperature densification of MEC-based ceramics. During sintering, low-melting-point Si can form a transient liquid phase that fills intergranular pores and promotes mass transport, consequently enhancing the

densification of MEC-based ceramics[22, 26, 28].

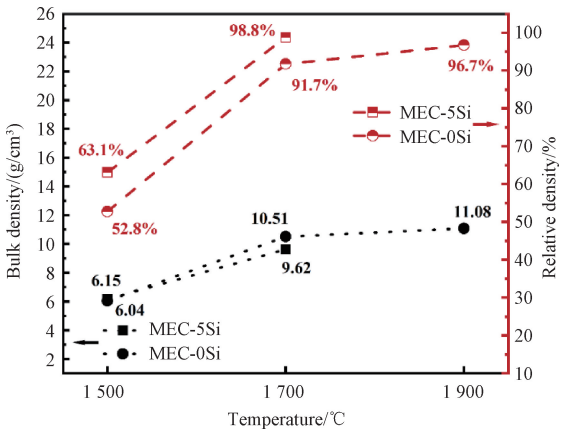

MEC-5Si—MEC with 5% Si; MEC-0Si—Si-free MEC.

Fig. 4 Bulk density and relative density of MEC-based ceramics sintered at different temperatures

2.2.3 Microstructure of MEC-based ceramics

Figure 5 shows the morphology and elemental distribution of the polished surface of the MEC-based ceramics. The Si-free MEC-0Si-1900 ceramic consists primarily of the MEC phase, with an average grain size of (3.8 ± 1.3) μm, and minor intergranular residual carbon. In contrast, the Si-added MEC-based ceramic, MEC-5Si-1700, exhibits a dual-phase structure, a gray matrix phase, and a black secondary phase. Based on the XRD and EDS analysis, the gray matrix phase and the black secondary phase are an MEC solid solution and in-situ-formed SiC, respectively. The MEC matrix grain size in MEC-5Si-1700 is refined to (1.4 ± 0.3) μm, which is merely 36.8% of that in MEC-0Si-1900. The results reveal that the addition of Si causes significant microstructural refinement of MEC-based ceramics. EDS mapping confirms the homogeneous distribution of Zr, Hf, and W in the matrix phase of the sintered MEC-based ceramics, with no evidence of elemental segregation. Based on the EDS and XRD results, it is confirmed that the reaction between Si and MEC not only preserves the crystal structure of the cubic carbide phase but also enhances solid solution formation by generating carbon vacancies. These vacancies accelerate atomic diffusion and reduce kinetic barriers for the formation of a homogeneous solid solution[29].

Notably, SiC particles display non-uniform distribution, which can be attributed to their formation mechanism. During RSPS, small-radius carbon atoms demonstrate higher diffusivity than Si atoms. They detach from transition metal carbide lattices and migrate toward Si particles to react with them, causing the in-situ formation of SiC with a distribution replicating the spatial arrangement of the original Si powder. These in-situ-formed SiC particles exert a pinning effect on MEC grain boundaries, inhibiting boundary migration and consequently suppressing matrix grain growth. Furthermore, the reduced densification temperature of RSPS for the Si-added MEC-based ceramics further suppressed grain growth thermodynamically. Thus, the second particle pinning effect and the low sintering temperature synergistically refine the microstructure during RSPS of MEC-based ceramics.

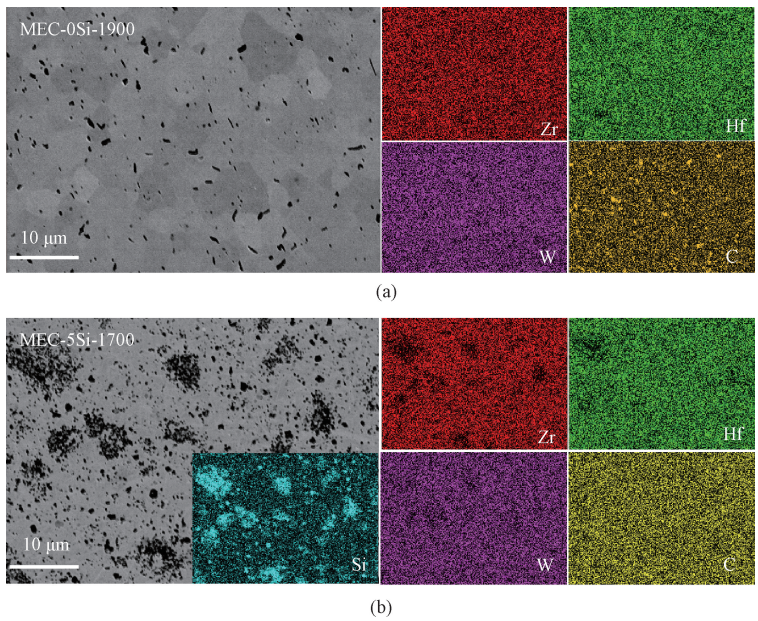

Fig. 5 SEM morphology and related EDS mapping images of MEC-based ceramics: (a) MEC-0Si-1900; (b) MEC-5Si-1700

2.3 Mechanical properties of MEC-based ceramics

Table 1 shows the key mechanical properties of MEC-based ceramics, including Young's modulus, Vickers hardness, and fracture toughness. The Young's moduli of the dense Si-added MEC-based ceramic and the dense Si-free MEC ceramic are very close. This is

primarily attributed to the combined effects of the relative density of the Si-added MEC-based ceramics, the elimination of residual carbon, and the reaction-generated SiC phase. On one hand, the addition of Si promotes the densification of MEC-based ceramics. The relative density of MEC-5Si-1700 ceramic is 2.1 percentage points higher than that of MEC-0Si-1900 ceramic. Additionally, the residual carbon with a low modulus at grain boundaries is eliminated in the former, which helps improve the Young's modulus of the material. On the other hand, the in-situ-formed SiC phase has a Young's modulus of approximately 400–420 GPa, which is lower than that of the MEC phase. According to the mixing rule, the presence of the SiC phase leads to a decrease in the overall Young's modulus of MEC/SiC composite ceramics. The comprehensive effect of the above factors results in the fact that the addition of 5% Si not significantly affect the Young's modulus of the MEC-based ceramics.

Table 1 Mechanical properties of MEC-based ceramics

Sample	E/GPa	$H_{V1.0}$/GPa	K_{IC}/(MPa·m$^{1/2}$)
MEC-0Si-1900	443±5	20.7±0.5	2.74±0.09
MEC-5Si-1700	440±3	21.6±0.5	3.42±0.24

The hardness of MEC-5Si-1700 increases by approximately 4.3% compared to MEC-0Si-1900. Based on the above-mentioned results on densification and microstructure, the addition of Si improves the relative density of MEC-based ceramics and eliminates the soft residual carbon at grain boundaries, thereby contributing to the enhancement of hardness. Meanwhile, the addition of Si induces grain refinement in the MEC-based ceramic matrix. According to the classical Hall-Petch relationship, grain refinement significantly hinders dislocation movement, resulting in a fine-grain strengthening effect that effectively enhances the hardness of MEC-based ceramics. In other words, adding Si into MEC leads to high relative density, elimination of residual carbon, and fine grains, which collectively enhance the hardness of MEC-based ceramics.

Compared with Si-free MEC ceramics, the addition of 5% Si significantly increases the fracture toughness of the material by approximately 24.8%, primarily attributed to the toughening effect of in-situ generated SiC secondary phase. During the failure process of MEC-based ceramics under the stress, when cracks encounter SiC secondary particles with different modulus and thermal expansion coefficient from the matrix MEC phase during propagation, the crack path (Fig. 6) deflects due to changes in the local stress field and the presence of interfaces[30]. This increases the crack propagation area, consumes more fracture energy, and thus significantly improves the fracture toughness of MEC-based ceramics.

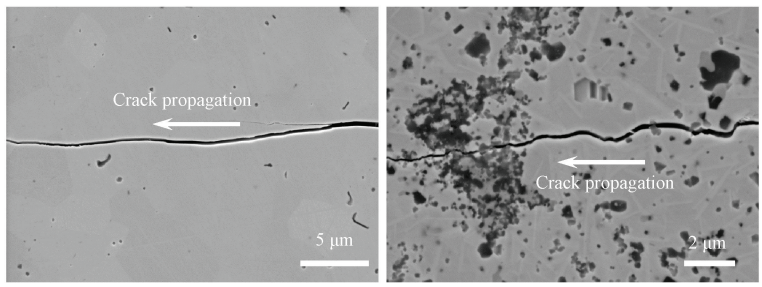

(a) (b)

Fig. 6 Crack propagation path in MEC-based ceramics: (a) MEC-0Si-1900; (b) MEC-5Si-1700

3 Conclusions

This study successfully achieved low-temperature densification and fracture toughness enhancement in medium-entropy $(Zr_{1/3}Hf_{1/3}W_{1/3})C$ ceramic by introducing Si additives combined with RSPS. Experimental results confirm that Si addition operates through a threefold mechanism.

1) Low-melting-point Si significantly promotes the densification by forming a transient liquid phase.

2) Reaction between Si and carbides generates abundant carbon vacancies, promoting atomic diffusion and facilitating the formation of medium-entropy $(Zr_{1/3}Hf_{1/3}W_{1/3})C$ solid solution. This reduces both densification and solid solution formation temperatures from 1 900 ℃ to 1 700 ℃.

3) In-situ-formed SiC particles effectively suppress the matrix grain growth via grain boundary pinning and enhance fracture toughness by approximately 24.8% through crack deflection.

Overall, the Si-assisted reactive sintering strategy validates effective microstructural control and performance enhancement in medium-entropy ceramics. This approach achieves simultaneous high relative density, grain refinement, and toughness improvement at temperatures below those required for medium-entropy ceramics, offering valuable insights for designing high-temperature carbide materials for extreme environments.

References

[1] WUCHINA E, OPILA E, OPEKA M, et al. UHTCs: ultra-high temperature ceramic materials

for extreme environment applications[J]. *The Electrochemical Society Interface*, 2007, 16(4): 30-36.
[2] NI D W, CHENG Y, ZHANG J P, et al. Advances in ultra-high temperature ceramics, composites, and coatings [J]. *Journal of Advanced Ceramics*, 2022, 11(1): 1-56.
[3] HE J M, ZHAO G L, LIU T W, et al. Overview of advanced sintering technologies for high-entropy ceramics[J]. *Journal of Ceramics*, 2024, 45(1): 32-45. (in Chinese)
[4] BAO W C, GUO X J, XIN X T, et al. Establishment of symbiotic structure with metal atomic-layer phase-separation in carbide ceramics [J]. *Journal of Inorganic Materials*, 2025, 40(1): 17-22. (in Chinese)
[5] CASTLE E, CSANÁDI T, GRASSO S, et al. Processing and properties of high-entropy ultra-high temperature carbides[J]. *Scientific Reports*, 2018, 8(1): 8609.
[6] LU K, LIU J X, WEI X F, et al. Microstructures and mechanical properties of high-entropy ($Ti_{0.2}Zr_{0.2}Hf_{0.2}Nb_{0.2}Ta_{0.2}$)C ceramics with the addition of SiC secondary phase[J]. *Journal of the European Ceramic Society*, 2020, 40(5): 1839-1847.
[7] LI J, HE L, PENG F, et al. Optimized process and superior toughness of a (HfNbTaTiW)C high entropy carbide ceramic [J]. *Ceramics International*, 2024, 50(18): 32129-32137.
[8] Wei X F, Liu J X, Li F, et al. High entropy carbide ceramics from different starting materials [J]. *Journal of the European Ceramic Society*, 2019, 39(10): 2989-2994.
[9] ZHANG R Z, REECE M J. Review of high entropy ceramics: design, synthesis, structure and properties [J]. *Journal of Materials Chemistry A*, 2019, 7(39): 22148-22162.
[10] WANG W L, SUN G X, SUN X N, et al. Electromagnetic wave absorbing properties of high-entropy transition metal carbides powders [J]. *Materials Research Bulletin*, 2023, 163: 112212.
[11] RASAKI S A, ZHANG B X, ANBALGAM K, et al. Synthesis and application of nano-structured metal nitrides and carbides: a review [J]. *Progress in Solid State Chemistry*, 2018, 50: 1-15.
[12] SUN W W, YANG Y, WANG Y W. High entropy carbide (ZrNbTiCr)C ceramic composite coating with fine grains fabricated by plasma spraying[J]. *Surface and Coatings Technology*, 2024, 478: 130459.
[13] LI Z T, WANG Z, WU Z G, et al. Phase, microstructure and related mechanical properties of a series of (NbTaZr)C-based high entropy ceramics[J]. *Ceramics International*, 2021, 47(10): 14341-14347.
[14] ZHANG P X, YE L, CHEN F H, et al. Stability, mechanical, and thermodynamic behaviors of (TiZrHfTaM)C (M = Nb, Mo, W, V, Cr) high-entropy carbide ceramics[J]. *Journal of Alloys and Compounds*, 2022, 903: 163868.
[15] LI X T, WEI Z F, ZU Y F, et al. Phase composition and electrochemical properties of ($Hf_{0.2}Zr_{0.2}Ta_{0.2}Mo_{0.2}Ti_{0.2}$)$B_2$ high-entropy ceramics [J]. *Journal of Ceramics*, 2023, 44(4): 688-694. (in Chinese)
[16] LI Z W, GONG W L, CUI H F, et al. (Zr, Hf, Nb, Ta, W)C-SiC composite ceramics: preparation via precursor route and properties[J]. *Journal of Inorganic Materials*, 2025, 40(3): 271-283. (in Chinese)
[17] YAN Z H, LIU J X, PENG P, et al. Oxidation resistance of equimolar multicomponent transition metal carbide solid solution [J]. *Advanced Ceramics*, 2024, 45(6): 541-557. (in Chinese)
[18] LIU Y P, TUO P, DAI F Z, et al. A highly deficient medium-entropy perovskite ceramic for electromagnetic interference shielding under harsh environment[J]. *Advanced Materials*, 2024, 36(28): e2400059.
[19] YANG Q Q, WANG X G, BAO W C, et al. Influence of equiatomic Zr/(Ti, Nb) substitution on microstructure and ultra-high strength of (Ti, Zr, Nb)C medium-entropy ceramics at 1 900 ℃ [J]. *Journal of Advanced Ceramics*, 2022, 11(9): 1457-1465.
[20] YANG Q Q, WANG X G, WU P, et al. Ultra-high strength medium-entropy (Ti, Zr, Ta)C ceramics at 1 800 ℃ by consolidating a core-shell structured powder[J]. *Journal of the American Ceramic Society*, 2022, 105: 823-829.
[21] DEMIRSKYI D, BORODIANSKA H, SUZUKI T S, et al. High-temperature flexural strength performance of ternary high-entropy carbide consolidated via spark plasma sintering of TaC, ZrC and NbC[J]. *Scripta Materialia*, 2019, 164: 12-16.
[22] WANG X G, ZHANG G J, XUE J X, et al. Reactive hot pressing of ZrC-SiC ceramics at low temperature [J]. *Journal of the American Ceramic Society*, 2013, 96(1): 32-36.
[23] XIANG H M, XING Y, DAI F Z, et al. High-entropy ceramics: present status, challenges, and a look forward [J]. *Journal of Advanced Ceramics*, 2021, 10(3): 385-441.
[24] DEMIRSKYI D, NISHIMURA T, SUZUKI T S, et al. High-temperature toughening in ternary medium-entropy ($Ta_{1/3}Ti_{1/3}Zr_{1/3}$)C carbide consolidated using spark-plasma sintering[J]. *Journal of Asian Ceramic Societies*, 2020, 8(4): 1262-1270.

[25] ZOU Q, LI Z, LI Y G, et al. Fabrication and characterization of medium-entropy carbide ceramics in low temperature sintering [J]. *International Journal of Applied Ceramic Technology*, 2023, 20(3): 1504-1511.
[26] QIN Y, LIU J X, PENG P, et al. Phase stability of W-containing high-entropy carbide with silicon addition at high temperatures [J]. *Ceramics International*, 2024, 50(18): 32007-32014.
[27] LIU J X, GUO L W, WU Y, et al. Lattice rigidity in high-entropy carbide ceramics with carbon vacancies [J]. *Journal of the American Ceramic Society*, 2023, 106(10): 5612-5619.
[28] LIN G W, LIU J X, QIN Y, et al. Low-temperature reactive sintering of carbon vacant high-entropy carbide ceramics with in-situ formed silicon carbide [J]. *Journal of the American Ceramic Society*, 2022, 105(4): 2392-2398.
[29] GUO L W, LIU J X, QIN Y, et al. The indentation load effect of hardness of non-stoichiometric high-entropy carbides ($Ti_{0.2}Zr_{0.2}Hf_{0.2}Nb_{0.2}Ta_{0.2}$) C_{1-x} [J]. *Advanced Ceramics*, 2024, 45(1/2): 170-176. (in Chinese)
[30] FENG L, FAHRENHOLTZ W G, HILMAS G E, et al. Densification, microstructure, and mechanical properties of ZrC-SiC ceramics [J]. *Journal of the American Ceramic Society*, 2019, 102(10): 5786-5795.

低温反应放电等离子烧结法原位合成碳化硅增韧中熵 $(Zr_{1/3}Hf_{1/3}W_{1/3})C$ 陶瓷

李梦飞，彭　湃，刘吉轩*，秦　渊，程伟强，张国军
东华大学 先进纤维材料全国重点实验室 材料科学与工程学院，上海 201620

摘　要：中熵过渡金属碳化物陶瓷及其复合材料是极端环境用重要耐高温材料，但其面临着致密化困难与断裂韧性低的挑战。针对这一问题，采用碳热还原法合成了名义成分为($Zr_{1/3}Hf_{1/3}W_{1/3}$)C(MEC)的中熵陶瓷粉体，然后添加 Si 并利用反应放电等离子烧结(RSPS)技术制备了 MEC 基复相陶瓷。研究发现，未添加 Si 时，MEC 陶瓷需在 1 900 ℃ 烧结才能形成单相固溶体，此时其相对密度和平均晶粒尺寸分别为 96.7%和(3.8 ± 1.3) μm。添加 5%(质量分数)Si 后，在 1 700 ℃烧结，可获得相对密度为 98.8%的 MEC 基复相陶瓷，其由 MEC 固溶体相和原位反应生成的 SiC 第二相构成。MEC 基体相的平均晶粒尺寸仅为(1.4 ± 0.3)μm。与单相 MEC 陶瓷相比，添加 Si 制备的 MEC 基复相陶瓷的断裂韧性提高了 24.8%，达(3.42 ± 0.24)MPa·$m^{1/2}$。分析认为，低熔点 Si 可在烧结过程中形成液相以促进致密化。同时，Si 与碳化物反应会导致后者内部形成碳空位，可加速原子扩散，促进 MEC 固溶体相的形成。另外，原位反应生成的 SiC 相不仅会钉扎基体相的晶界，阻碍其生长，还能引起裂纹偏转，提高材料的断裂韧性。该研究结果可为极端环境用新型中熵碳化物基陶瓷的设计与制备提供参考。

关键词：中熵碳化物；碳热还原反应；反应烧结；碳化硅；增韧